Identification of projectile sequential decay and incomplete fusion in the $^{16}O+^{28}Si$, $^{16}O+^{27}Al$, and $^{10}B+^{27}Al$ systems at 4–5 MeV/nucleon

N. Carlin Filho, M. M. Coimbra, N. Added, R. M. dos Anjos, L. Fante, Jr.,
M. C. S. Figueira, V. Guimarães, E. M. Szanto, and A. Szanto de Toledo
Instituto de Física da Universidade de São Paulo, Departamento de Física Nuclear, Laboratório Pelletron, 01498, São Paulo, São Paulo, Brazil

O. Civitarese
Departamento de Física, Universidad Nacional de La Plata, 1900, La Plata, Argentina
(Received 26 October 1988)

In-plane angular correlations have been investigated in the $^{28}Si(^{16}O,^{12}C\ \alpha)$, $^{27}Al(^{16}O,^{12}C\ \alpha)$, and $^{27}Al(^{10}B,^{6}Li\ \alpha)$ reactions at 64, 64, and 48 MeV, respectively. Two sequential processes have been clearly identified, namely, projectile sequential decay and incomplete fusion followed by particle reemission. The analysis is based on three-body kinematics and model fits of experimental angular correlation functions.

Over the last few years studies of light-particle emission were used to probe early stages of heavy-ion reaction mechanisms yielding both to inclusive and coincidence data. There has been increasing interest in unambiguous identification of projectile fragmentation, preequilibrium emission, and incomplete fusion mechanisms.[1–4] The controversy found in the literature concerning the identification of these mechanisms and their competition in light systems[5–7] reflects the experimental difficulties and calls for alternative and systematic studies. The $^{27}Al(^{16}O,^{12}C\alpha)$ system has received most of the attention, although no conclusive interpretation has been drawn. While some authors pointed out the dominance of α-transferlike processes followed by preequilibrium[5] decay, others suggested the occurrence of incomplete fusion processes.[6,7] A different approach, which still does not allow for a clear identification, has been adopted by Sasagase *et al.*[8] by tentatively postulating out the coexistence of two different sequential processes. Therefore systematic studies, based on exclusive measurements which reveal projectile and target dependence of these mechanisms, are necessary in order to establish a unified picture for sequential processes in light heavy-ion reactions.

In this study we present results on the investigation of the $^{28}Si(^{16}O,^{12}C\alpha)$, $^{27}Al(^{16}O,^{12}C\alpha)$, and $^{27}Al(^{10}B,^{6}Li\alpha)$ reactions. The experiments were performed using ^{16}O ($E_{lab}=64$ MeV), and ^{10}B ($E_{lab}=48$ MeV) beams supplied by the University of São Paulo Pelletron accelerator. Self-supporting ^{27}Al (1 mg cm^{-2}), and ^{nat}Si (750 μg cm^{-2}) targets were used. Carbon and lithium particles were identified with a 2.3 msr solid angle telescope consisting of a 15 μm ΔE and a 1 mm E solid state detector fixed at $+30°$ and $+20°$, respectively. Alpha particles in coincidence were detected, in the reaction plane, at angles varying from $-100°$ to $+60°$, using three (ΔE-E) telescopes ($\Delta E=20$ μm, $E=2$ mm), each subtending a 5 msr solid angle. At forward angle measurements, the elastically scattered particles were suppressed by using thin Ta absorbers (≈ 50 mg cm^{-2}) located in front of the light-particle detectors.

Experimental angular correlation functions are shown in Fig. 1. These functions have well-defined maxima at forward negative angles, and are asymmetric. It is important to note that one of the systems investigated, namely $^{27}Al(^{16}O,^{12}C\alpha)$ at 64 MeV, has been previously measured by Harris *et al.*[5] and Tsang *et al.*,[6] and that these two measurements disagree significantly. In the first case the angular correlation peaks at $\theta_\alpha^{lab}\approx -40°$, while in the second case the maximum is found at $\theta_\alpha^{lab}\approx -10°$. The angular correlation function for the $^{27}Al(^{16}O,^{12}C\alpha)$ system, obtained in the present work, is consistent with the data from Tsang *et al.*[6] The observed asymmetry could, in principle, be attributed to contributions from different processes. In order to characterize these contributions we have performed kinematical and model analysis. The first allows verification of the existence of an intermediate state in the sequential processes, and the second permits determination of the mechanism by which the intermediate state has been populated. The following three-body processes were considered:

(a) Projectile sequential decay (PSD):

$$^{16}O+^{28}Si\rightarrow{}^{16}O^*+^{28}Si\rightarrow{}^{12}C+\alpha+^{28}Si\ ,$$

$$^{16}O+^{27}Al\rightarrow{}^{16}O^*+^{27}Al\rightarrow{}^{12}C+\alpha+^{27}Al\ ,$$

$$^{10}B+^{27}Al\rightarrow{}^{10}B^*+^{27}Al\rightarrow{}^{6}Li+\alpha+^{27}Al\ .$$

(b) Incomplete fusion (ICF):

$$^{16}O+^{28}Si\rightarrow{}^{12}C+{}^{32}S^*\rightarrow{}^{12}C+\alpha+^{28}Si\ ,$$

$$^{16}O+^{27}Al\rightarrow{}^{12}C+{}^{31}P^*\rightarrow{}^{12}C+\alpha+^{27}Al\ ,$$

$$^{10}B+^{27}Al\rightarrow{}^{6}Li+{}^{31}P^*\rightarrow{}^{6}Li+\alpha+^{27}Al\ .$$

Total energy spectra were constructed on the basis of a three-body final state kinematics consisting of a light-ion (L denotes alpha particle), a heavy-ion (H denotes ^{12}C or ^{6}Li), and a residual nucleus (R denotes ^{28}Si or ^{27}Al) (see Fig. 2). Derived Q-value spectra based on the relation

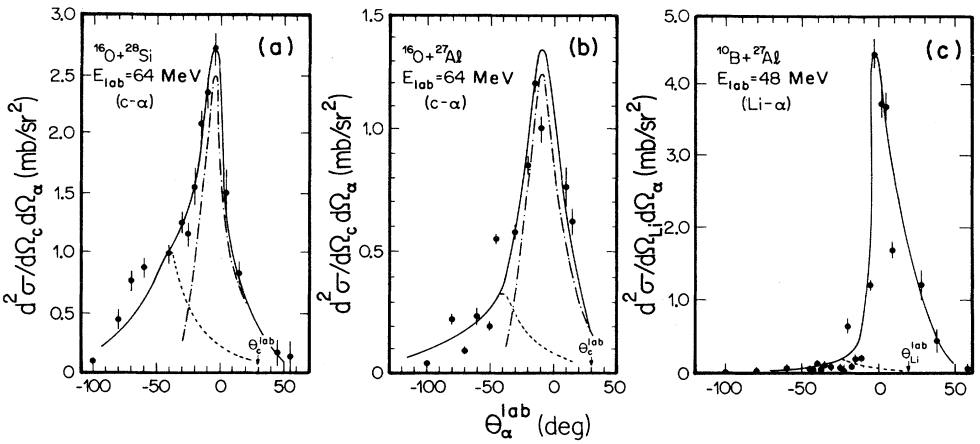

FIG. 1. In-plane angular correlation functions for (^{12}C-α) and (^{6}Li-α) products measured at $\theta_C = +30°$, $\theta_{Li} = +20°$. Fits based on ICF and PSD mechanisms are shown by dashed and dash-dotted lines, respectively. Total contributions are indicated by solid lines.

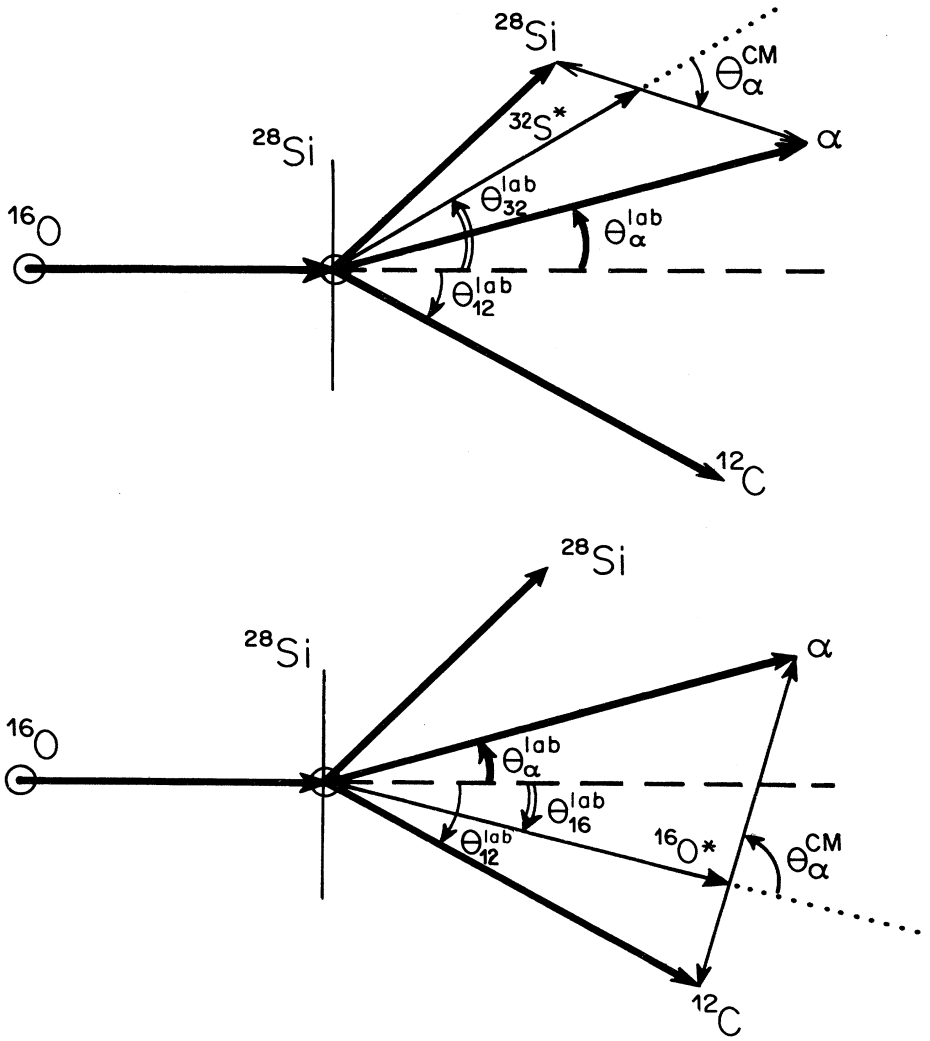

FIG. 2. Schematic velocity diagram for the ^{28}Si(^{16}O,^{12}Cα) reaction showing ICF (upper) and projectile sequential decay PSD (lower).

$$Q = E_L + E_H + E_R - E_{\text{projectile}}$$

indicate that most of the events correspond to final state configurations with all three products (L, H, and R) in their ground state [see Fig. 3(a)].

Kinetic energies of relative motion E^{rel}_{L+H}, E^{rel}_{L+R}, or E^{rel}_{H+R} between $(L+H)$, $(L+R)$, or $(H+R)$ pairs of particles, were also obtained for all the events [e.g., see Fig. 3(b)] in the case of the $^{10}B+^{27}Al$ system. Figure 4 shows the average values (E^{rel}_{L+R} and E^{rel}_{L+H}) for the relative kinetic energies calculated for all angular configurations. These values are seen to be constant at negative backward angles ($\theta_\alpha < -40°$) only in the $(L+R)$ cases, i.e., (α-^{28}Si) and (α-^{27}Al) pairs (represented by filled circles), thus indicating that the intermediate nucleus $^{32}S^*$ ($^{31}P^*$) was formed and the incomplete fusion (ICF) process is dominant at $\theta^{\text{lab}}_\alpha \leq 40°$.

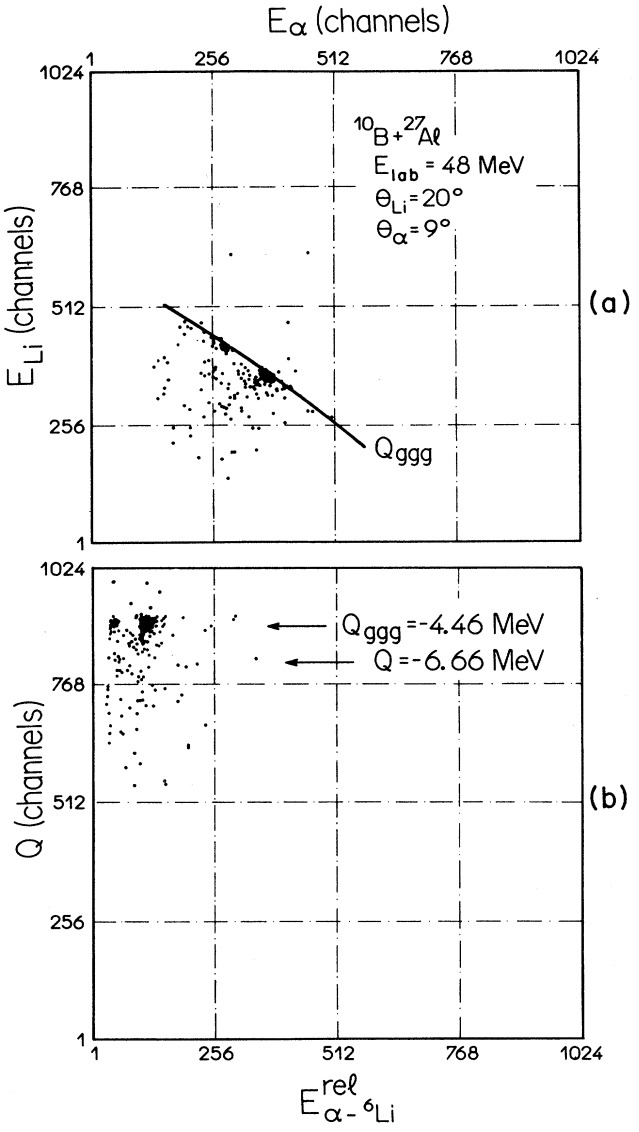

FIG. 3. (a) Two-dimensional representation of the coincidence events, for the $^{27}Al(^{10}B,^6Li\alpha)$ reaction, as a function of the E_{Li} and E_α energies. The solid line labeled Q_{ggg} describes the expected trajectory of the events corresponding to final configurations with all three products ($^{27}Al,^6Li,\alpha$) in their ground state. (b) Q value vs E^{rel}_{L+H} spectrum derived from the part (a). Events corresponding to the [^{27}Al(g.s.), ^{6}Li(g.s.),α] and [^{27}Al(g.s.), ^{6}Li*(3^+,2.185 MeV),α] configurations are identified by their respective Q values, i.e., $Q_{ggg} = -4.46$ MeV and $Q_{gg1} = -6.66$ MeV, respectively.

On the other hand, in the angular range where the E^{rel}_{L+R} varies, ($\theta > -30°$), the relative energies referred to the $^{16}O^*$ ($^{10}B^*$) rest frame for the α-^{12}C (α-^{6}Li) breakup configuration (described by empty circles) tend slowly to a constant value (especially in the B+Al system). This constancy is not always evident due to the kinematical limitations imposed on the angular observation range which suppress the contribution of some of the excited states in ^{16}O (^{10}B). In other words, the average excitation energy of the recoiling intermediate nucleus is not strictly constant due to the contribution of different states at different angles. It should be mentioned that there exist well-defined peaks associated with the projectile excited states in the relative energy spectra (see Fig. 5), at all α-particle detection angles ($\theta_\alpha > -30°$), whose average energies are affected by the predicted kinematical limits indicated by the horizontal dashed lines in Fig. 4. These results suggest the presence of an intermediate stage which leads to the subsequent projectile decay (PSD).

The constant values of E^{rel}_{L+R} at $\theta_\alpha < -40°$, extracted from Fig. 4 allow one to infer values of the average excitation energy E^*_{IN} of the intermediate nucleus $^{32}S^*$ ($^{31}P^*$) prior to the α emission (see Table I).

On the other hand, the observation of discrete states in the relative energy spectra E^{rel}_{L+H}, for the $\theta_\alpha > -20°$ angular region, which can be associated to excited states of the $^{16}O^*$ ($^{10}B^*$) intermediate nucleus, supports the picture of a breakup process.

Once the presence of a sequential process is established, complementary information on the reaction mechanism can be obtained by means of model analysis of the angular correlation functions, which permits identification of the process responsible for the intermediate nucleus formation. In the case of the ICF process the first stage is described by the fusion of an α particle with a Si (Al) target. The excitation energies and recoil angles of the intermediate nuclei IN$\equiv$[$^{32}S^*$ ($^{31}P^*$)] are derived from the experimental kinetic energies of the projectile remnants ^{12}C (^{6}Li) at $\theta^{\text{lab}}_c = +30°$ ($\theta^{\text{lab}}_{\text{Li}} = +20°$). The probability ($d\sigma/dE^*_{\text{IN}}$) for the population of a given state in the intermediate nucleus in associated with the experimental double differential cross section

$$\sum_{\theta_\alpha} \frac{d^2\sigma}{d\Omega\, dE_H} \equiv \frac{d^2\sigma}{d\Omega\, dQ_H} \propto P(Q_H, \theta_H) ,$$

which generates the $^{32}S^*$ ($^{31}P^*$) spectra. The excited $^{32}S^*$ ($^{31}P^*$) nucleus will evaporate an α particle with an angular distribution given by the Hauser-Feshbach (HF) statistical theory $(d\sigma/d\Omega)^{\text{HF}}_\alpha(Q_H, \theta_H, \theta_\alpha)$ calculated with the code STATIS.[10] Within this picture, this Hauser-Feshbach cross section must be weighted by the probabil-

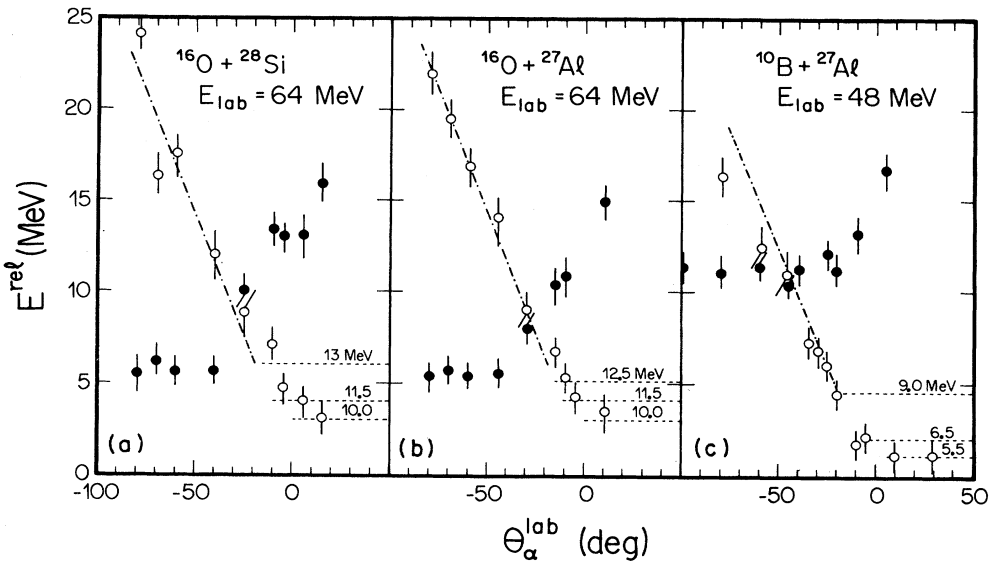

FIG. 4. Relative kinetic energies E^{rel}_{L+R} [i.e., $E^{rel}_{\alpha\text{-Si}}(E^{rel}_{\alpha\text{-Al}})$] (full circles) and E^{rel}_{L+H} [i.e., $E^{rel}_{\alpha C}(E^{rel}_{\alpha Li})$] (empty circles) as a function of the α particle detection angles. Dashed horizontal lines indicate the kinematically allowed angular interval for quoted projectile excited states $^{16}O^*$ (or $^{10}B^*$). If the relative energies of the $(L+H)$ pair is calculated using values of E_H, E_L, and E_R obtained from a hypothetical decay of the intermediate $^{32}S^*$ ($^{31}P^*$) nucleus, whose excitation energy is taken from Table I, they will lie on the dot-dashed line.

ity of forming a ^{32}S (E^*_{32},θ_{32}) [^{31}P (E^*_{31},θ_{31})] nucleus, as given by the experimental double differential cross section $(d^2\sigma/d\Omega\, dQ_H)=P(Q_H,\theta_H)$ where Q represents the Q value for the first step in the ICF process.

Determination of the initial angular momentum values of the states in $^{32}S^*$ ($^{31}P^*$) was based on the picture of the fusion of an α particle with the ^{28}Si (^{27}Al) target for the bombarding energy needed to reproduce the observed $^{32}S^*$ ($^{31}P^*$) excitation energy. The sharp cutoff approximation has been used in all the calculations.

The resulting ICF angular correlation is written as

$$\left[\frac{d^2\sigma}{d\Omega_H d\Omega_\alpha}(\theta_\alpha^{lab})\right]_{ICF} = \sum_{Q_H} P(Q_H,\theta_H)\left[\frac{d\sigma}{d\Omega}\right]^{HF}_{\alpha}(Q_H,\theta_H,\theta_\alpha^{lab}) . \quad (1)$$

No free parameters were admitted in these calculations. The parameters used in the statistical model calculations indicated in Fig. 6 were extracted from the literature for this mass region.[9] The effect of the variation of these parameters in the predicted angular correlation can be visualized in Fig. 6, where it may be seen that the position of the peak of the angular correlation is insensitive to these variations, and is determined basically by the recoil angle of the intermediate $^{32}S^*$ ($^{31}P^*$) nucleus.

For the PSD process, the observed ^{12}C (^6Li) nucleus is not produced in the first step, and consequently, for each ^{12}C (^6Li) kinetic energy value, a set of scattering angles and excitation energies of the ^{16}O (^{10}B) particles is admitted using kinematical considerations. In this case, the ^{12}C (^6Li) spectra were used individually to calculate the probability distribution for the $^{16}O^*$ ($^{10}B^*$) scattering of the intermediate nucleus at the corresponding angle

TABLE I. Values of the excitation energies observed in the ICF and PSD process.

System	E_{lab} (MeV)	ICF E^*_{IN} (MeV)[a]	ICF $Q_{optimum}$ (MeV)	ICF E^*_{opt} (MeV)[c]	ICF E^*_{IF} (MeV)[d]	PSD E^*_p (MeV)[e]
$^{16}O+^{28}Si$	64	$E^*_{^{32}S^*}=12.5\pm1.0$	−10.7	10.5	19.2	$E^*_{^{16}O}=9.7,10.4,11.5,13.0,15.0$
$^{16}O+^{27}Al$	64	$E^*_{^{31}P^*}=15.0\pm1.0$	−10.5	13.0	21.6	$E^*_{^{16}O}=9.7,10.4,11.5,13.0,15.0$
$^{10}B+^{27}Al$	48	$E^*_{^{31}P^*}=21.7\pm1.0$	−15.7	20.9	24.9	$E^*_{^{10}B}=5.2,5.6,6.0,7.0$

[a]Most probable excitation energy for the intermediate nucleus obtained using the relative energies from Fig. 4.
[b]Optimum Q value for an α-transfer reaction.
[c]Most probable excitation energy (E^*_{opt}) for the intermediate nucleus obtained on the basis of a $Q_{optimum}$ value for the α transfer.
[d]Expected excitation energy for a fusion process of a beam velocity α particle taking into account the binding energies.
[e]Excitation energy of the projectile prior to the breakup.

$\theta_{\text{projectile}}$ [see Fig. 2(b)]. Therefore, the angular correlation function is obtained from the sum of the product of two factors. The first

$$P(\theta_p, Q_p) = (d^2\sigma / d\Omega_p dQ_p) ,$$

where the subscript p refers to the projectile, is related to the probability of scattering the projectile at an angle θ_p with an excitation energy $E_p^* = -Q_p$. The second factor refers to the $^{16}O^*$ ($^{10}B^*$) intermediate nucleus decay probability into the α-^{12}C (^6Li) channel at the observed angle $(\theta_H, \theta_\alpha)$. According to the above hypothesis, the PSD angular correlation can be written as

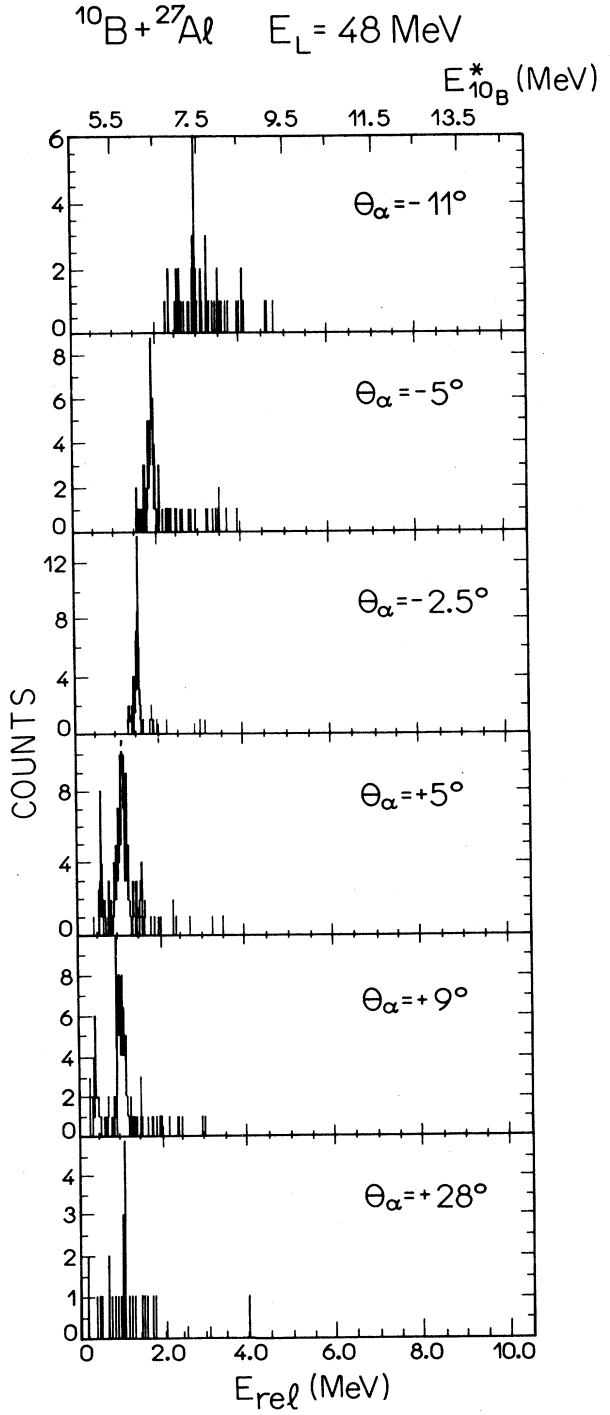

FIG. 5. Spectra of relative energies $E^{\text{rel}}_{\text{Li-}\alpha}$ for the $^{27}Al(^{10}B,^6Li\alpha)$ reaction at several angular configurations.

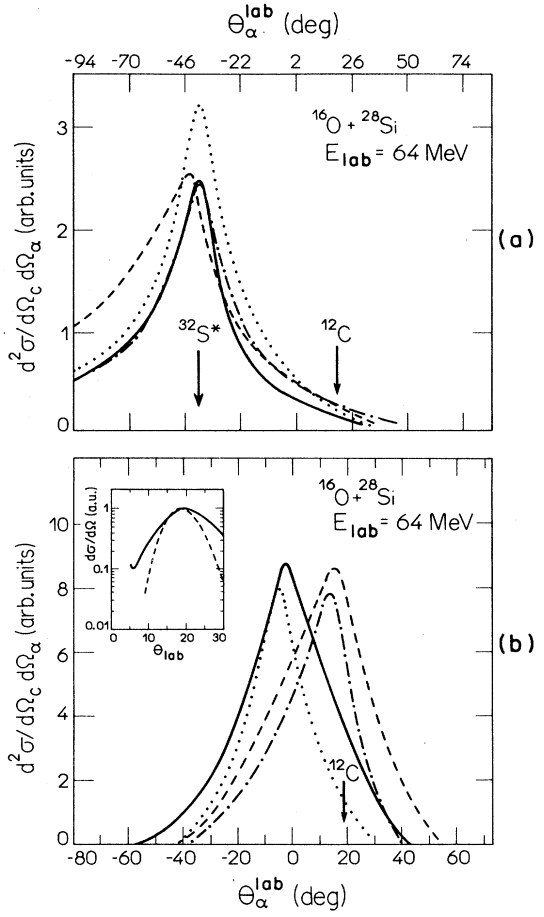

FIG. 6. Predicted angular correlations for the $^{28}Si(^{16}O,^{12}C\alpha)^{28}Si$ system for (a) incomplete fusion process: (i) level density parameter $a = A/8$, critical angular momentum for the fusion of $\alpha + ^{28}Si$, $J_{\text{crit}} = 30\hbar$ and Q-value distribution of $P(Q_H, \theta_H)$ obtained from the ^{12}C experimental spectra (solid line) (this parametrization has been used in Fig. 1); (ii) same parameters as (i) with Q-value distribution shifted artificially by +3 MeV, i.e., $P[(Q_H + 3 \text{ MeV}), \theta_H]$, (dashed line); (iii) same as (i) with level densities given by Gilbert and Cameron (Ref. 11) (dotted line); (iv) same as (i) with $J_{\text{crit}} = 12\hbar$ (dot-dashed line). The inferred $^{32}S^*$ recoiling angle is indicated by an arrow. (b) projectile sequential decay: (i) $\theta_0 = 20°$ and $\sigma = 7\sigma$ (solid line), (ii) $\theta_0 = 20°$ and $\sigma = 4°$ (dotted line), (iii) $\theta_0 = 24°$ and $\sigma = 7°$ (dashed line), (iv) $\theta_0 = 24°$ and $\sigma = 4°$ (dot-dashed line). The carbon detection angle is also indicated. Figure inset: prediction of coupled-channel calculations $^{28}Si[^{16}O,^{16}O^*(11.6 \text{ MeV})]$ for the inelastic scattering (solid line) and the Gaussian approximation (dashed line) utilized for the $P_p(\theta_p, Q)$ distribution, described by its centroid θ_0 and width σ.

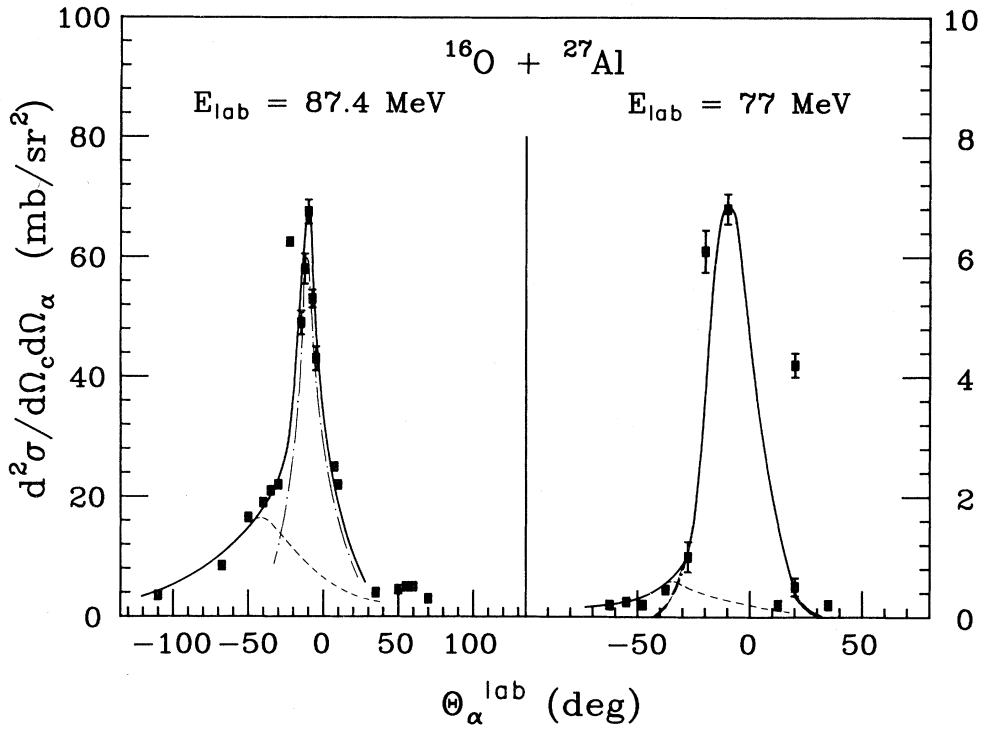

FIG. 7. Angular correlation functions for the $^{16}O+^{27}Al$ systems from Ref. 7 ($E_L=77$ MeV) and Ref. 8 ($E_L=87.4$ MeV). Curves represent fits using expressions (2) and (3) with the same parameters as Fig. 1.

$$\left[\frac{d^2\sigma}{d\Omega_H d\Omega_\alpha}(\theta_\alpha^{\rm lab})\right]_{\rm PSD} = \sum_{E_H}\sum_{\theta_p}\sum_{Q_p} P_p(\theta_p,Q_b)\frac{d^2\sigma}{d\Omega_H dE_H}(\theta_\alpha)\ , \quad (2)$$

where E_H denotes the energy of the heavy projectile-like final fragment.

The projectile inelastic scattering cross section $P_p(\theta_p,Q_p)$ was calculated by using the shape of the angular distribution predicted by coupled-channel calculations. To simplify the computation of the angular correlation function, $P_p(\theta_p,Q_p)$ was approximated by two adjacent semi-Gaussians centered at a θ_0 angle near the grazing angle. This approximation allows identification in a simple way of the main parameters which define the shape of the angular correlation associated with the PSD process. The two semi-Gaussian widths $\sigma_<$ and $\sigma_>$ as well as θ_0 were taken as free parameters. It may be seen that the values used in the present calculation are very similar to those predicted by the coupled-channels calculation based on the code ECIS (Ref. 12) [see insert in Fig. 6(b)].

The experimental angular correlation functions were χ^2 fitted by the incoherent sum of the contribution of both ICF and PSD processes by means of the relation

$$\left[\frac{d^2\sigma(\theta_\alpha^{\rm lab})}{d\Omega_H d\Omega_\alpha}\right]_{\rm total}^{\rm exp} = a\left[\frac{d^2\sigma}{d\Omega_H d\Omega_\alpha}(\theta_\alpha^{\rm lab})\right]_{\rm ICF} + b\left[\frac{d^2\sigma}{d\Omega_H d\Omega_\alpha}(\theta_\alpha^{\rm lab})\right]_{\rm PSD}\ , \quad (3)$$

where a and b are normalizing parameters. The best fits are shown by the solid lines in Fig. 1.

It should be noted that, regarding the ICF process, the experimental values for the $^{32}S^*$ ($^{31}P^*$) excitation energies listed in Table I are consistent with expected values for a direct α transfer with an optimum Q value (see Table I). This result indicates that a direct transfer with subsequent emission of an α particle most likely occurs in the first stage of the reactions rather than the process of a beam velocity α particle fusing with the target.

Contributions due to ICF processes in which the heavy fragment is transferred and subsequently reemitted were found to be negligible, in comparison to the other two processes considered here. This result can be easily understood in terms of the reduction of exit channel Coulomb barrier penetrabilities, the very low Q values involved and the expected inhibition of the correlation function for the angular position of the particle detectors. The results of the present analysis are summarized as follows:

(i) The angular dependence of relative energies clearly points out the existence of a sequential reaction mecha-

nism.

(ii) The fit of the angular correlation functions allows for the identification of the presence of two different processes, namely, incomplete fusion and projectile sequential decay.

Fits of the data available in the literature for the $^{16}O+^{27}Al$ system[7,8] (see Fig. 7) reinforce these conclusions. The comparison of our results, for the $^{27}Al(^{16}O,^{12}C\alpha)$ system, with other studies of the same system, leads to the following comments: With respect to the conflicting data and interpretations between Harris *et al.*[5] and Tsang *et al.*,[16] this work agrees with the latter author. Our results differ from those Ref. 7 in that although the presence of an ICF process was identified in our work, the main structure in the angular correlation originates from a PSD process.

Concerning the influence of nuclear structure effects upon ICF and PSD processes, we can conclude that while ICF results show only a slight target dependence, PSD results display a strong projectile dependence. It should also be noted that the results shown in Fig. 5 suggest that the present technique might be a convenient tool for studying cluster structure in light heavy nuclei.

ACKNOWLEDGMENTS

This work was partly supported by Conselho Nacionale de Desenvolvimento Científico e Tecnologico (CNPq), Brazil, by Fundação de Amparo a Pesquisa do Estado de São Paulo (FAPESP), Brazil, and Consejo Nacional de Investigaciones Científicas y Tecgnologicas (CONICIT), Argentina.

[1]P. L. Gonthier, H. Ho, M. N. Namboodiri, J. B. Natowitz, L. Adler, S. Simon, K. Hagel, S. Kniffen, and A. Khodai, Nucl. Phys. **A411**, 289 (1983); H. Ho, P. L. Gonthier, G. Y. Fan, W. Küan, A. Pfoh, L. Schad, R. Wolski, J. P. Wurm, J. C. Adlogg, D. Disdier, A. Kamili, V. Rauch, G. Rudolf, F. Scheibling, and A. Strazzeri, Phys. Rev. C **27**, 584 (1983).

[2]W. D. M. Rae, A. J. Cole, B. G. Harvey, and R. G. Stokstad, Phys. Rev. C **30**, 158 (1984).

[3]R. K. Browmik, J. Van Driel, R. H. Siemssen, G. J. Balster, P. B. Goldhoorn, S. Gongrijp, Y. Iwasaki, R. V. F. Janssens, H. Sakai, K. Siwek-Wilczynska, W. A. Starrenburg, and J. Wilczynski, Nucl. Phys. **A390**, 117 (1982).

[4]H. Morgenstern, W. Bohne, W. Galster, and K. Grabisch, Z. Phys. A **324**, 443 (1986).

[5]J. W. Harris, T. M. Cormier, D. F. Geesaman, L. L. Lee, Jr., R. L. McGrath, and J. P. Wurm, Phys. Rev. Lett. **38**, 1460 (1977).

[6]M. B. Tsang, W. G. Lynch, R. J. Puigh, R. Vandenbosch, and A. G. Seamster, Phys. Rev. C **23**, 1560 (1981).

[7]S. J. Padalino and L. C. Dennis, Phys. Rev. C **31**, 1794 (1985).

[8]M. Sasagase, M. Sato, S. Hanashima, K. Furuno, Y. Magashima, Y. Tagishi, S. M. Lee, and T. Mikuno, Phys. Rev. C **27**, 2630 (1983).

[9]N. Carlin Filho, M. M. Coimbra, J. C. Acquadro, R. Liguori Neto, E. M. Szanto, E. Farrelly-Pessoa, and A. Szanto de Toledo, Phys. Rev. C **31**, 152 (1985).

[10]R. G. Stokstad, Yale University Wright Nuclear Structure Laboratory Report **52**, 1972.

[11]A. Gilbert and A. G. W. Cameron, Can. J. Phys. **43**, 1446 (1965).

[12]J. Raynal, *Optical Model and Coupled Channel Calculation in Nuclear Physics* (IAEA, Vienne, 1972).